Phase Current Reconstruction and Control of Three-Phase Switched Reluctance Machine With Modular Power Converter Using Single DC-Link Current Sensor

Shoujun Song, *Senior Member, IEEE*, Zekun Xia, *Student Member, IEEE*, Gaoliang Fang, Ruiqing Ma, *Member, IEEE*, and Weiguo Liu, *Senior Member, IEEE*

***Abstract*—According to the modular power converter, a novel phase current reconstruction method using single dc-link current sensor is proposed for three-phase switched reluctance machine (SRM), and the control method is implemented with the reconstructed phase current as well. A highly integrated modular power converter is constructed by a three-phase full bridge and a dual switch module. The phase windings are in star-connection, and the bipolar phase currents are applied. Based on the special operating modes and single pulse width modulation signal injection, the dc-link current is decoupled and the phase current in both magnetization and demagnetization regions is reconstructed, which is very critical for the implementation of some advanced methods that require complete period phase current. The conventional control methods of the SRM, such as single-pulse voltage and hysteresis current control methods, are carried out under different operating conditions with both simulation and experiment to verify the effectiveness of the proposed method, and the reconstruction errors and performance influences are detailed analyzed as well.**

***Index Terms*—Complete current period, control method, modular configuration, phase current reconstruction, power converter, single current sensor, switched reluctance machine (SRM).**

I. Introduction

In RECENT years, the more/all electric aircrafts, electric vehicles (EVs) and hybrid EVs are becoming promising transportation options due to the increasing energy crisis and environmental concerns [1]–[4]. Switched reluctance machine (SRM), which has no rotor windings and permanent magnets, achieves simple structure, low cost, excellent high-speed capability, and harsh environment applicability, and is a competitive candidate for more/all electric transportation applications [5]–[8].

For SRM drive system, its cost, weight, and size mainly depend on the power converter and the sensors without counting the machine. Recently, some approaches were presented to improve the integration level of the SRM drive systems. For the power converter, some standard industrial switch modules were applied [9]–[12]. In [9], a conventional three-phase full-bridge inverter was used to drive a 6/4-pole SRM, whose windings were in star-connection. This simple topology is good for reducing the noise and torque ripple. However, two phases must be simultaneously energized, which sacrifices the control flexibility, and limits the torque output and speed range of the system [10], [11]. In [12], a three-phase full-bridge inverter was adopted to drive a 12/10-pole SRM. The configuration reduces the number of switches and connections between converter and machine, but the current level of all switches is doubled. In [13], a multiport power converter was used to minimize the bus capacitor. This converter only requires two switch modules, but it is hard to control owing to the multiplexed switches and coupled controlled variables. In [14], a modular converter constructed by one dual and one three-phase full-bridge switch module was proposed. The phase windings are in star-connection and bipolar current waveform was applied, but overlapping conduction is forbidden in the control method, which results in low average torque and big torque ripple. In [15], novel operating modes were proposed and the basic control schemes were enhanced to improve the performances with the converter mentioned in [14], and the dynamic performances of the SRM are compared with the conventional asymmetric half-bridge (AHB) converter. However, detailed analysis about the differences of the phase currents between the modular and AHB converter are not involved.

Concerning the simplicity and cost of sensor circuits, efforts were made mainly from two aspects. Position sensorless control is a widely studied issue [16]–[19]. Without the position sensors, namely optical encoder, hall sensor and resolver, the reliability of the drive systems increases especially under harsh environment. The other hot topic is current sensor number

Manuscript received April 7, 2017; revised July 17, 2017 and October 21, 2017; accepted November 25, 2017. Date of publication December 11, 2017; date of current version July 15, 2018. This work was supported by the Xi'an Science and Technology Plan under Grant 2017086CG/RC049(XBGY002), the Aeronautical Science Foundation of China under Grant 2015ZB53018, and the Fundamental Research Funds for the Central Universities under Grant 3102017AX007. Recommended for publication by Associate Editor Y. Sozer. *(Corresponding author: Shoujun Song.)*

S. Song, G. Fang, R. Ma, and W. Liu are with the Department of Electrical Engineering, Northwestern Polytechnical University, Xi'an 710072, China (e-mail: sunnyway@nwpu.edu.cn; fanggaoliang@mail.nwpu.edu.cn; marq@nwpu.edu.cn; lwglll@nwpu.edu.cn).

Z. Xia is with the McMaster Institute for Automotive Research and Technology, McMaster University, Hamilton, ON L8S 4K1, Canada (e-mail: xiaz9@mcmaster.ca).

Color versions of one or more of the figures in this paper are available online at http://ieeexplore.ieee.org.

Digital Object Identifier 10.1109/TPEL.2017.2782562

See http://www.ieee.org/publications_standards/publications/rights/index.html for more information.

reduction, particularly for the low-power drive systems, where the cost and size are important criteria. This issue was discussed mainly for ac machines, and various techniques have been proposed [20]–[25]. For commonly used voltage-source inverter of ac machines, the pulse width modulation (PWM) signals are regulated to detect all phase currents from the bus current in the whole control periods [20], [21]. For the ac machines fed by direct matrix converter, single current sensor was adopted to reconstruct the phase current based on the space vector modulation [22]. In [23], a new technique to reconstruct the phase currents using a bus current sensor was presented, and an observer was built to generate stable three-phase responses, even the information of the phase current is not reflected in the bus. In [24], with a neutral-point current sensor, a new space vector PWM scheme was presented to estimate phase currents in three-level T-type converter. In [25], a new reconstruction method was proposed to expand the sampling area of the phase current.

Phase current reconstruction of SRM was presented in [26] for the first time. The proposed converter topology makes it easy to separate the demagnetization current from the bus current, but the method was complex and not very effective. In [27], the same converter circuit in [26] was adopted, and double high-frequency pulses were injected into the lower switches of the bridge arms for current reconstruct. The reconstructed phase currents tracked the actual sampled currents with a good agreement, and hysteresis current control (HCC) method using the reconstructed phase currents was implemented to verify the dynamic performance. In [28], based on the phase current reconstruction method in [27], a low-cost torque control technique was proposed. However, due to the special converter topology in [27] and [28], the phase current in demagnetization region cannot be obtained, which results in performance degradation of some advanced methods that require complete current waveform [29]. Furthermore, the standard switch modules were not considered. In [30], phase currents of SRM were reconstructed by solving the linear equations associated with two adjacent phase currents in the different turn-on regions. The method is free from power transistor open-circuit fault, and current sensor offset was considered. It is a new point of view to reconstruct the phase currents. However, two current sensors are required.

All the aforementioned works about phase current reconstruction of SRM did not concern modularization of power converter and implementation of control methods simultaneously. In this paper, these two issues are both considered. Based on the special excitation modes and PWM signal injection technology, a new phase current reconstruction method of the SRM driven by the highly integrated modular converter in [14] and [15] is proposed. The method just requires one dc-link current sensor, and can obtain the complete period phase current, including both the magnetization and demagnetization region. Detailed simulations and experiments are carried out to demonstrate the effectiveness of the proposed method.

The rest of the paper is organized as follows. The adopted modular power converter and its operating modes are described in Section II. Section III proposes the phase current reconstruction method. In Sections IV and V, the effectiveness of the phase current reconstruction scheme with the modular power converter is verified with detailed simulation and experiment, respectively, and the reconstruction errors and performance influences of the proposed method are discussed as well. Section VI concludes the paper.

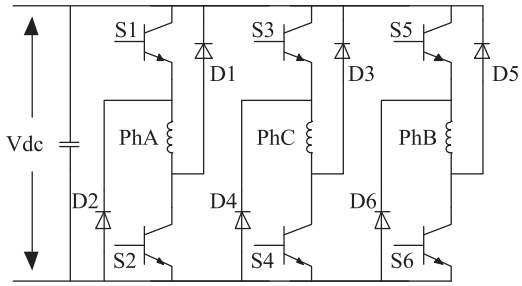

Fig. 1. 3-phase AHB converter.

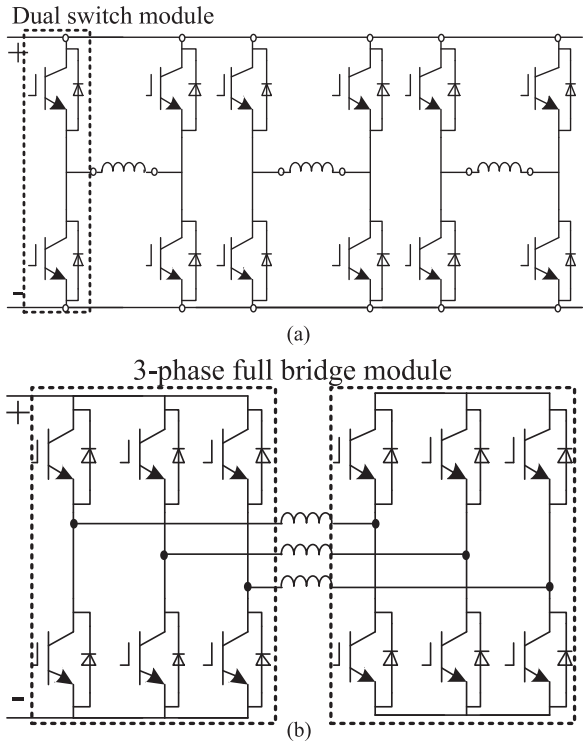

Fig. 2. Two modular configurations of AHB converter: (a) Using six dual modules and (b) Using two three-phase full-bridge modules.

II. Modular Converter and Operating Modes

Because of the control flexibility and no requirement on extra resistance or reactance components, the AHB converter is wildly used in many applications [31]. There are two switches and two diodes per phase and each branch can be independently controlled, as illustrated in Fig. 1.

In general, discrete components are used to build the AHB converter. However, several standard switch modules were also adopted, as shown in Fig. 2 [32], [33]. From the figure, it can be found that, just half of the components are used when the phase windings are unipolar excited, which decreases the utilization rate of the modules.

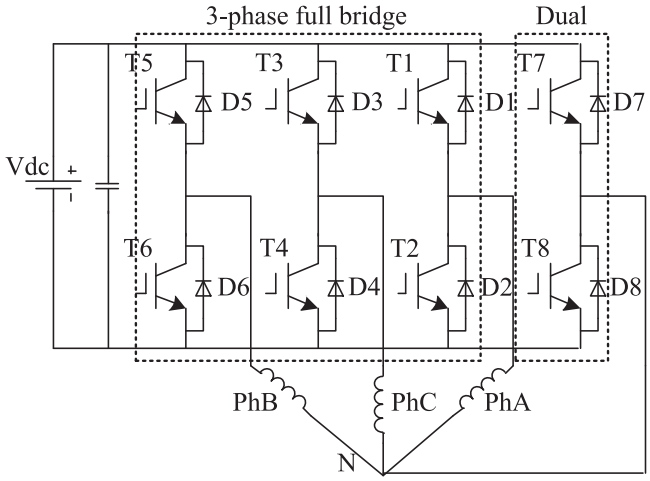

Fig. 3. Adopted modular converter for three-phase SRM.

A. Modular Converter

The modular converter adopted in this paper is implemented by a dual and a three-phase full-bridge switch module, and phase windings are connected in star with a neutral line, as illustrated in Fig. 3 [14]. This topology also can be conveniently constructed by other combinations of standard industrial switch modules, for example, two four-pack switch modules or four dual switch modules. Switch modules are widely adopted in the industrial applications, such as the three-phase full-bridge modules for the drive systems of ac machines. Therefore, it is convenient to choose the modules with appropriate voltage and current levels, and the cost is relatively low because of mass production.

For a three-phase SRM, if only discrete components are considered, the AHB converter requires six switches and six diodes, while the adopted modular converter needs eight switches and eight diodes, which means that the AHB converter is cheaper in terms of power devices. However, it should be noted that the main purposes of converter construction with switch modules are to reduce system complexity, increase the integration and reliability, and enhance the flexibility of component selection and converter construction.

B. Operating Modes

Magnetization, freewheeling, and demagnetization are three operating modes of the conventional AHB converter, as shown in Fig. 4. According to the analysis of the modular converter in [15], there are two forms for each operating mode, namely single phase and two phases in series, and the current directions of two neighboring phases are reverse when energized simultaneously, as shown in Fig. 5. Fig. 6 shows the phase currents and switching logic of a three-phase SRM with AHB and modular converter under HCC method, where θ is the rotor position and i is the phase current. It can be seen that the phase currents for the AHB converter are unidirectional, while bidirectional for the modular converter. It should be noted that the direction that the current flowing into the neutral point N is considered as positive.

In [15], it was concluded that although the phase windings of the considered modular converter are in Y-connection, due

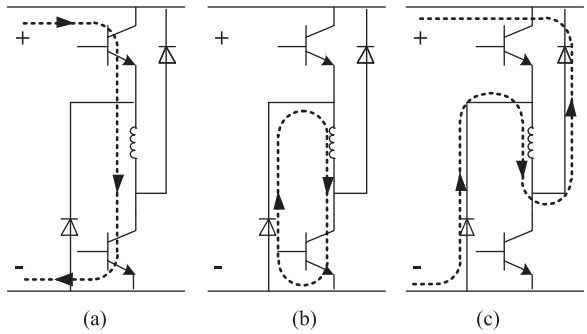

Fig. 4. Operating modes of the AHB converter. (a) Magnetization. (b) Freewheeling. (c) Demagnetization.

to the existence of the neutral line and dual switch module, each phase can be independently controlled, which makes the modular converter has similar performances, such as average torque per ampere ratio, torque ripple coefficient and efficiency, to the conventional AHB converter. Furthermore, because of the phase independence, the fault-tolerant ability of the modular converter is as good as the AHB converter. For example, if open-circuit fault occurs to one phase, the output power can be maintained by increasing the current of other two normal phases.

III. Proposed Phase Current Reconstruction Method

The phase current information plays a critical role in many control methods of the SRM, such as HCC method and direct instantaneous torque control (DITC) method. For HCC method, the real phase currents need to be compared with the reference current. For DITC method, all phase currents are required for instantaneous torque estimation. However, the existence of the current sensors will increase the weight, size, cost, and complexity, and decrease the reliability of the drive system. Therefore, it has great significance to research on the method that can reduce the number of the current sensors. In this section, the relationship among the dc-link and phase currents of the considered modular converter is analyzed first, and then, a new phase current reconstruction method with single dc-link current sensor is proposed.

A. Current Relationship

In Fig. 7, according to the rotor position, seven regions are created for current relationship analysis, and i_a, i_b, and i_c represent the current of phase A, B, and C, respectively. The position of the dc-link current sensor is shown in Fig. 8, and the dc-link current is denoted as $i_{\rm dc}$. Taking phase A as an example, the relationships between i_a and $i_{\rm dc}$ in different regions are detailed analyzed as follows.

In region I, phase B has been excited, and phase A is at the beginning of the excitation. Due to the existence of the phase windings, both the current of phase A and B cannot suddenly changed, so at the beginning of this situation, $-i_b$ is bigger than i_a, and their difference, namely $-i_b - i_a$, need find its own loop which has low impedance. According to the analysis of the circuit, $-i_b - i_a$ will circulate through the neutral line and D8,

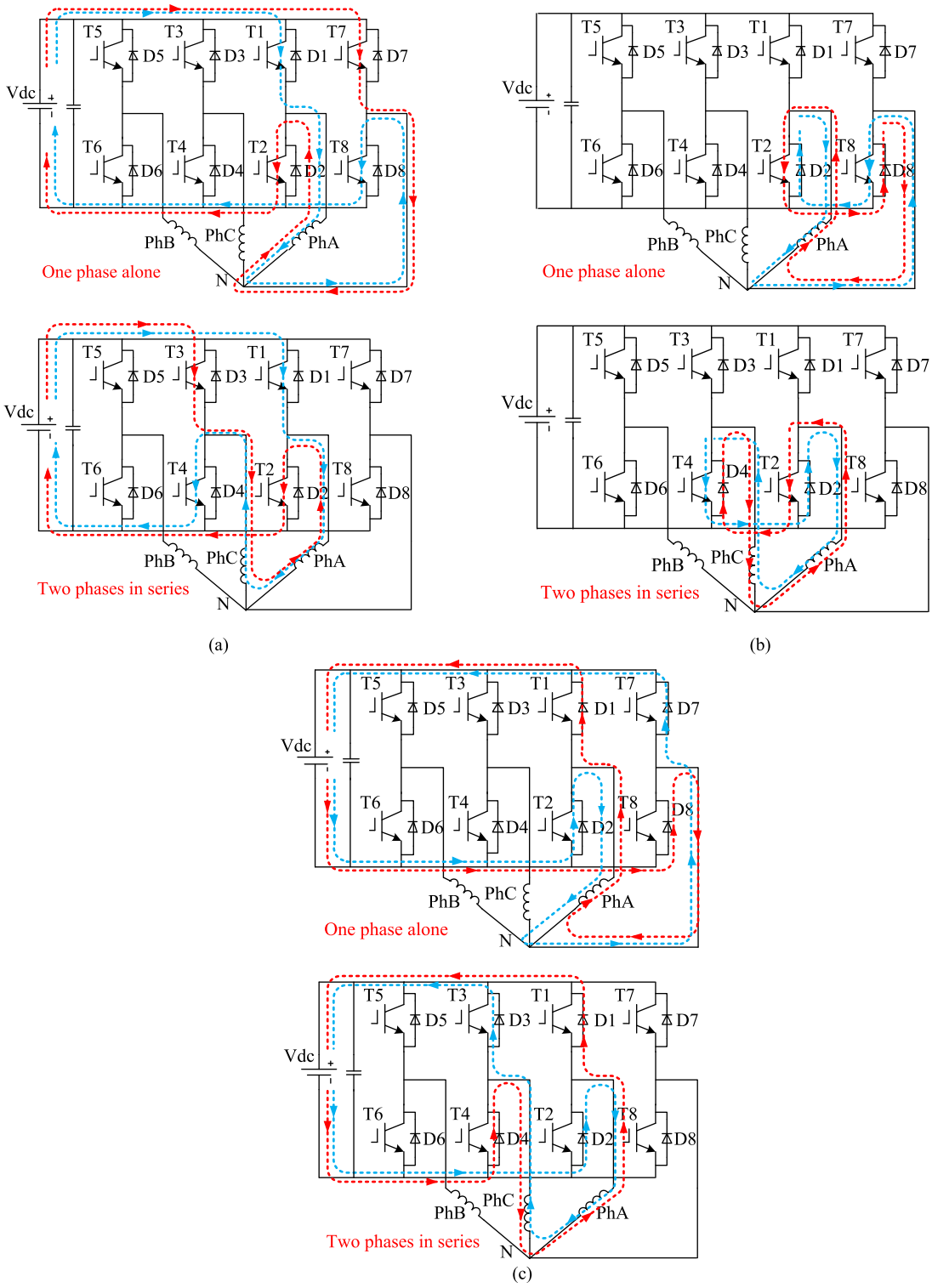

Fig. 5. Operating modes of the considered modular converter. (a) Magnetization. (b) Freewheeling. (c) Demagnetization.

and can be denoted as i_N. The current flow is shown in Fig. 9(a), and in this region, the dc-link current can be expressed as

$$i_{\rm dc} = i_a \quad (\theta_{{\rm on}A} \le \theta < \theta_1) \tag{1}$$

where $\theta_{{\rm on}A}$ represents the turn-on angle of phase A, and θ_1 denotes the rotor position where $|i_a| = |i_b|$.

It should be noted that in the above analysis, the negative sign in front of i_b is resulted from the current direction definition.

In region II, i_N becomes 0, and $-i_b = i_a$. In this case, only one current loop exists. Fig. 9(b) shows the current flow, and the dc-link current can be expressed as

$$i_{\rm dc} = i_a = -i_b \quad (\theta_1 \le \theta < \theta_{{\rm off}B}) \tag{2}$$

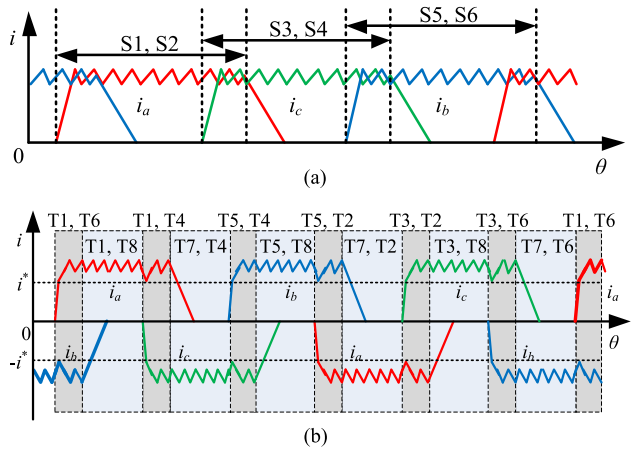

Fig. 6. Phase currents and switching logic of three-phase SRM with AHB and modular converter. (a) AHB converter. (b) Modular converter.

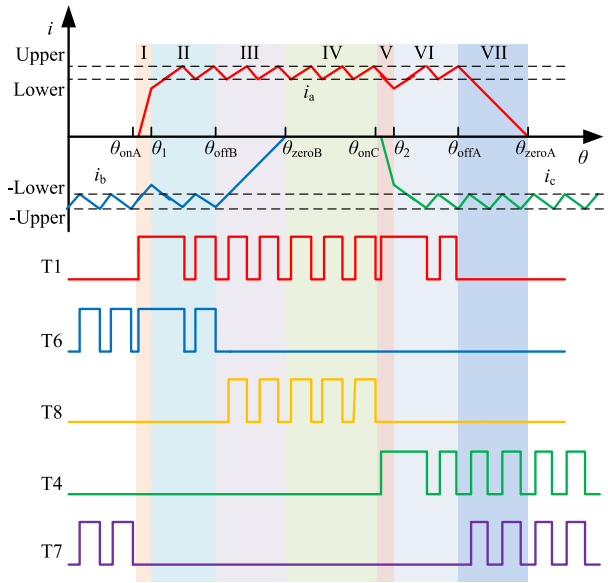

Fig. 7. Seven regions for the current of phase A.

where $\theta_{\mathrm{off}B}$ represents the turn-off angle of phase B.

In region III, phase A is magnetized alone through switches T1 and T8, while phase B demagnetized through diode D5. Fig. 10(a) shows the current flow, and the dc-link current can be expressed as

$$i_{\mathrm{dc}} = -i_N = i_a - (-i_b) = i_a + i_b \quad (\theta_{\mathrm{off}B} \le \theta < \theta_{\mathrm{zero}B}) \tag{3}$$

where $\theta_{\mathrm{zero}B}$ is the rotor position, where i_b decreases to zero.

It should be noted that the existence of i_N is because of the difference between $-i_b$ and i_a.

In region IV, the current of phase B equals to zero, and the winding of phase A is still magnetized. Fig. 10(b) shows the current flow, and the dc-link current can be expressed as

$$i_{\mathrm{dc}} = i_a \quad (\theta_{\mathrm{zero}B} \le \theta < \theta_{\mathrm{on}C}) \tag{4}$$

where $\theta_{\mathrm{on}C}$ represents the turn-on angle of phase C.

In region V, phase A has been excited, and phase C is at the beginning of the excitation. Due to the existence of the phase

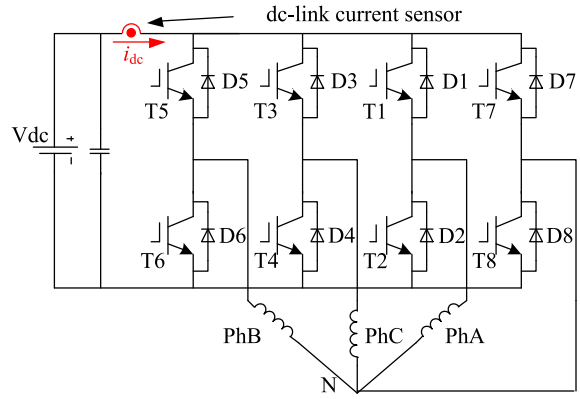

Fig. 8. Position of the dc-link current sensor.

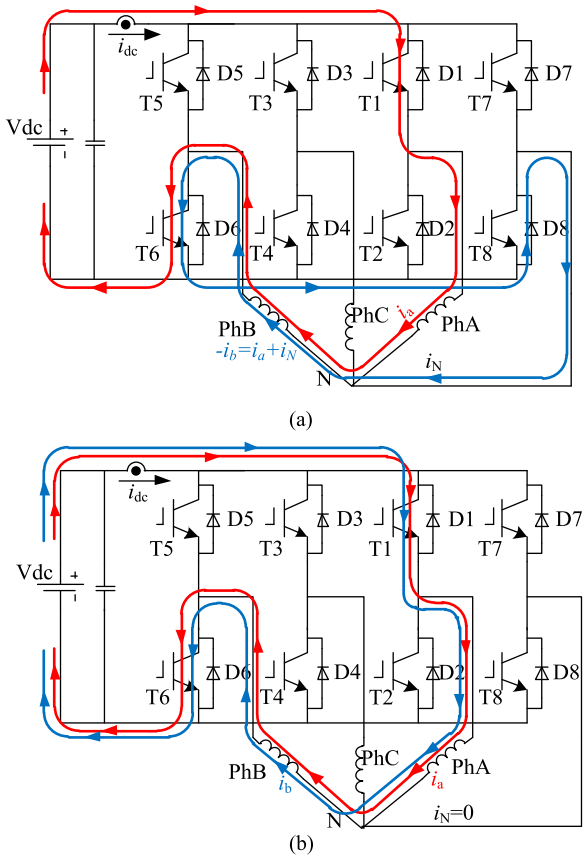

Fig. 9. Current flow in region I and II. (a) Region I. (b) Region II.

windings, both the current of phase A and C cannot suddenly changed, so at the beginning of this situation, i_a is bigger than $-i_c$, and their difference, namely $i_a - (-i_c)$, need find its own loop which has low impedance. According to the analysis of the circuit, $i_a - (-i_c)$ will circulate through the neutral line and D7, and can be denoted as $-i_N$. The current flow is shown in Fig. 11(a), and in this region, the dc-link current can be expressed as

$$i_{\mathrm{dc}} = -i_c \quad (\theta_{\mathrm{on}C} \le \theta < \theta_2) \tag{5}$$

where θ_2 denotes the rotor position, where $|i_a| = |i_c|$.

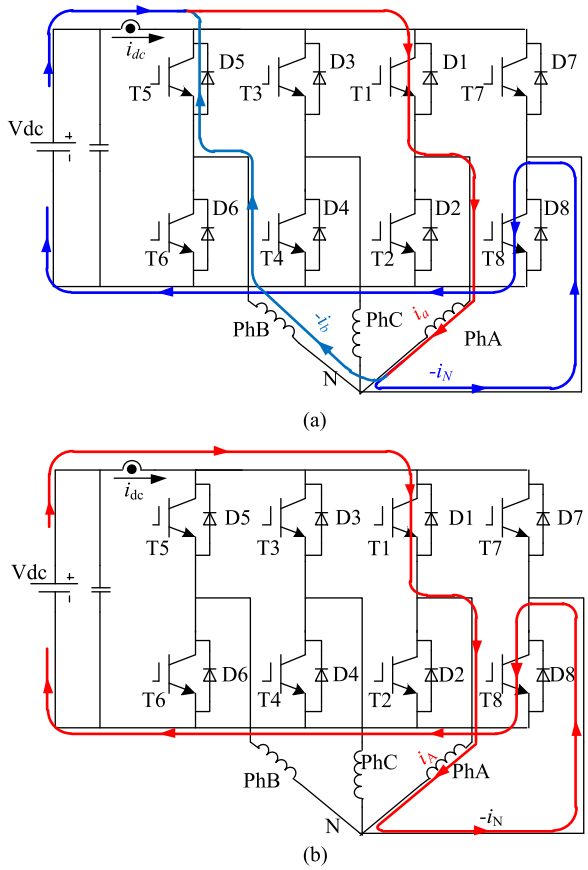

Fig. 10. Current flow in region III and IV. (a) Region III. (b) Region IV.

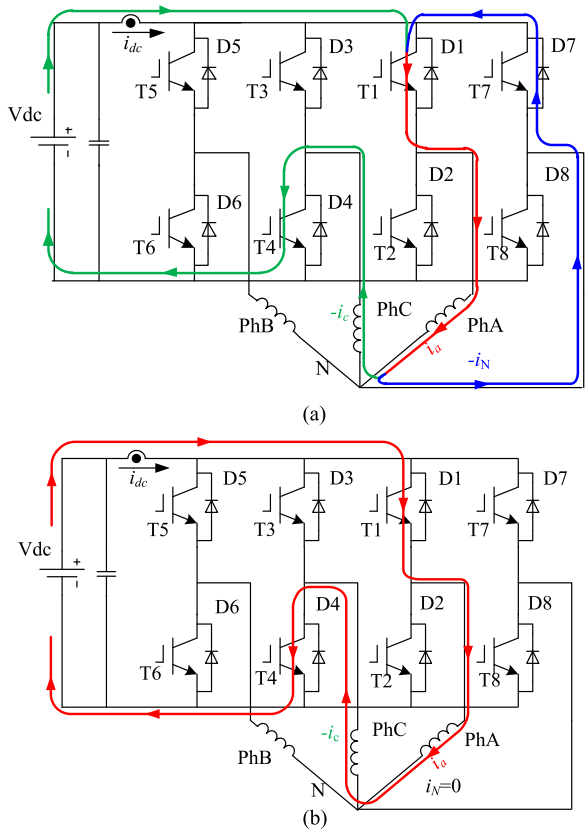

Fig. 11. Current flow in region V and VI. (a) Region V. (b) Region VI.

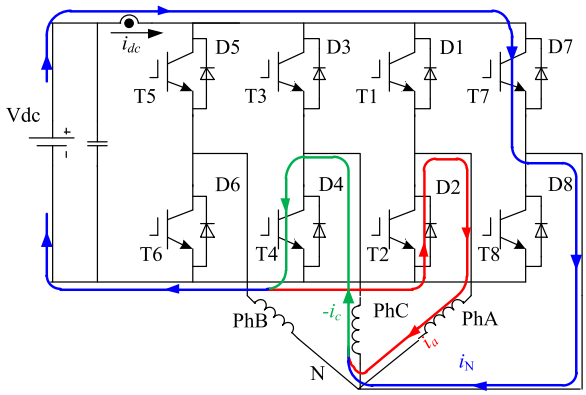

Fig. 12. Current flow in region VII.

In region VI, i_N becomes 0, and $i_a = -i_c$. In this case, only one current loop exists. Fig. 11(b) shows the current flow, and the dc-link current can be expressed as

$$i_{\mathrm{dc}} = i_a = -i_c \quad (\theta_2 \le \theta < \theta_{\mathrm{off}A}) \tag{6}$$

where $\theta_{\mathrm{off}A}$ represents the turn-off angle of phase A.

In region VII, phase C is magnetized alone through switches T4 and T7, while phase A is demagnetized through diode D2. Fig. 12 shows the current flow, and the dc-link current can be expressed as

$$i_{\mathrm{dc}} = -i_c - i_a \quad (\theta_{\mathrm{off}A} \le \theta < \theta_{\mathrm{zero}A}) \tag{7}$$

where $\theta_{\mathrm{zero}A}$ is the rotor position, where i_a decreases to zero.

In summary, i_{dc} can be expressed as (8) in the interval $[\theta_{\mathrm{on}A}, \theta_{\mathrm{zero}A}]$

$$i_{\mathrm{dc}} = \begin{cases} i_a & (\theta_{\mathrm{on}A} \le \theta < \theta_1) \\ i_a = -i_b & (\theta_1 \le \theta < \theta_{\mathrm{off}B}) \\ i_a + i_b & (\theta_{\mathrm{off}B} \le \theta < \theta_{\mathrm{zero}B}) \\ i_a & (\theta_{\mathrm{zero}B} \le \theta < \theta_{\mathrm{on}C}) \\ -i_c & (\theta_{\mathrm{on}C} \le \theta < \theta_2) \\ i_a = -i_c & (\theta_2 \le \theta < \theta_{\mathrm{off}A}) \\ -i_c - i_a & (\theta_{\mathrm{off}A} \le \theta < \theta_{\mathrm{zero}A}). \end{cases} \tag{8}$$

It should be noted that θ_1, θ_2, $\theta_{\mathrm{zero}A}$, and $\theta_{\mathrm{zero}B}$ are just used for the above analysis, and only the turn-on and turn-off angles are required for the implementation of the proposed method.

B. Phase Current Reconstruction Method

According to the above analysis about the relationship among i_{dc} and the phase currents, it can be found that i_{dc} directly equals to one phase current in some regions. For other regions, i_{dc} is the function of two phase currents. To decouple the dc-link current and reconstruct the phase currents, a pulse, for example, a large duty ratio PWM signal, is injected into appropriate switches of the converter in several regions. According to (8), the switches used to inject the PWM signal for current reconstruction of phase A in the interval $[\theta_{\mathrm{on}A}, \theta_{\mathrm{zero}A}]$ are shown in Table I and Fig. 13. It can be found that only region III, V, and VII require PWM injection.

TABLE I
SWITCHING LOGIC AND SWITCHES USED FOR PWM SIGNAL INJECTION

Regions	Rotor position	Switching logic	Switches used for PWM signal injection
I	$\theta_{on A} \le \theta < \theta_1$	T1 and T6	No
II	$\theta_1 \le \theta < \theta_{off B}$	T1 and T6	No
III	$\theta_{off B} \le \theta < \theta_{zero B}$	T1 and T8	T1 and T8
IV	$\theta_{zero B} \le \theta < \theta_{on C}$	T1 and T8	No
V	$\theta_{on C} \le \theta < \theta_2$	T1 and T4	T8
VI	$\theta_2 \le \theta < \theta_{off A}$	T1 and T4	No
VII	$\theta_{off A} \le \theta < \theta_{zero A}$	T7 and T4	T7 and T4

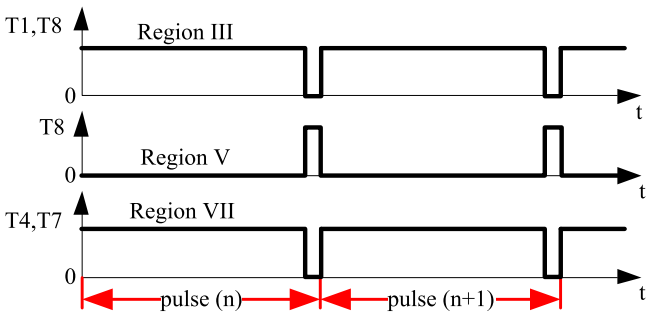

Fig. 13. PWM signal injected for current reconstruction of phase A.

In region III, phase B is demagnetized while phase A is energized, and i_b decreases. When the switches T1 and T8 are turned OFF, phase A begins to be demagnetized through two paths. One is through diodes D2 and D7, and the other one is through diodes D2, phase B winding and D5, as illustrated in Fig. 14(a). In this case, i_a can be written as

$$i_a = -i_N + (-i_b) = -i_{\rm dc} \tag{9}$$

where i_N is the current flowing through the neutral line.

In region V, phase C and A are simultaneously energized as shown in Fig. 11(a). When the switch T8 is turned ON, there are two paths for phase A magnetization. One is through switches T1 and T8, and the other one is through switches T1, phase C winding and switch T4, as shown in Fig. 14(b). In this case, i_a can be written as

$$i_a = -i_N + (-i_c) = i_{\rm dc}. \tag{10}$$

In region VII, phase C is magnetized alone and phase A is demagnetized. The relationship among phase A and C currents and the dc-link current is shown in (7). When the switches T4 and T7 are turned OFF, there are two paths for the demagnetization of phase C. One is through diodes D8 and D3, and the other one is through diode D2, phase A winding and diode D3, as shown in Fig. 15. In this state, $i_{\rm dc}$ is equal to i_c, and the relationship among currents can be written as

$$-i_{\rm dc} = -i_c = i_a + i_N. \tag{11}$$

As shown in Fig. 13, when pulse (n) is at low level, the dc-link current can be calculated as

$$-i_{\rm dc}(n) = -i_c(n) = i_a(n) + i_N(n). \tag{12}$$

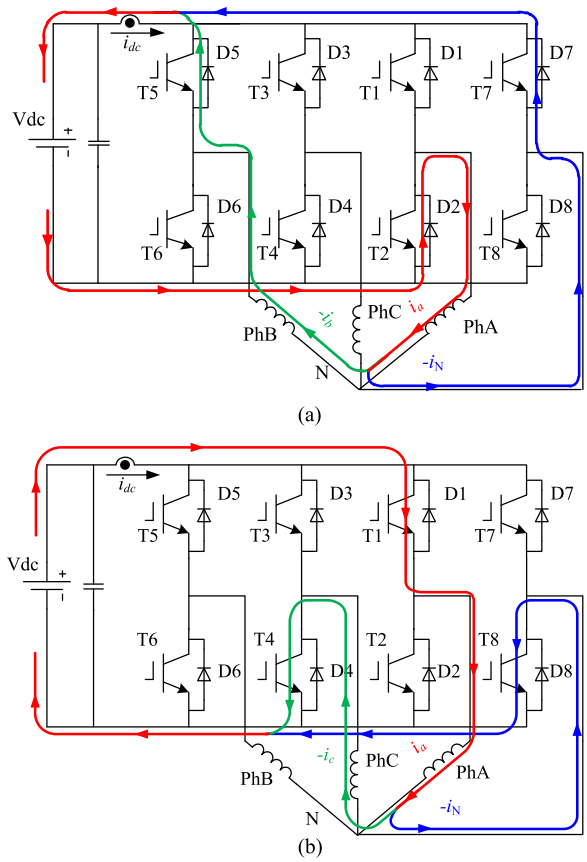

Fig. 14. Current flow in regions III and V with PWM injection. (a) Region III. (b) Region V.

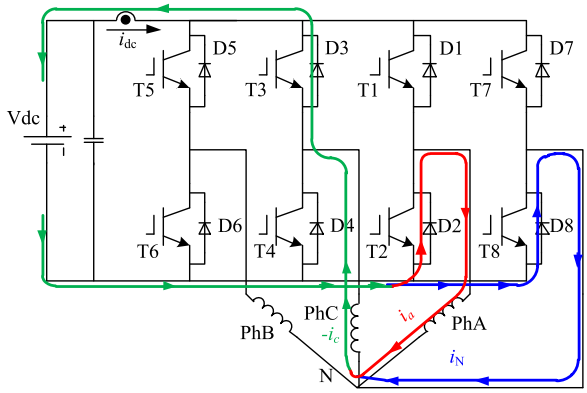

Fig. 15. Current flow in region VII with PWM injection.

When pulse (n+1) is at high level, according to (7), the dc-link current can be written as

$$i_{dc}(n+1) = -i_c(n+1) - i_a(n+1). \tag{13}$$

Based on (12) and (13), the current of phase A can be approximately obtained as

$$\begin{aligned} i_a(n+1) &= -i_c(n+1) - i_{\rm dc}(n+1) \\ &\approx -i_c(n) - i_{\rm dc}(n+1) \\ &\approx -i_{\rm dc}(n) - i_{\rm dc}(n+1). \end{aligned} \tag{14}$$

TABLE II
SWITCHING LOGIC, SWITCHES USED FOR PWM INJECTION, AND DC-LINK CURRENT WITH AND WITHOUT PWM INJECTION

Conduction phases	B, A	A	A, C	C	C, B	B	B, A	A	A, C	C	C, B	B
Switching logic	T1, T6	T1, T8	T1, T4	T7, T4	T5, T4	T5, T8	T5, T2	T7, T2	T3, T2	T3, T8	T3, T6	T7, T6
Switches used for PWM signal injection	T7	T1, T8	T8	T7, T4	T7	T5, T8	T8	T7, T2	T7	T3, T8	T8	T7, T6
dc-link current without PWM injection	i_a	$i_a + i_b$	$-i_c$	$-i_c - i_a$	i_b	$i_b + i_c$	$-i_a$	$-i_a - i_b$	i_c	$i_c + i_a$	$-i_b$	$-i_b - i_c$
dc-link current with PWM injection	$-i_b$	$-i_a$	i_a	i_c	$-i_c$	$-i_b$	i_b	i_a	$-i_a$	$-i_c$	i_c	i_b

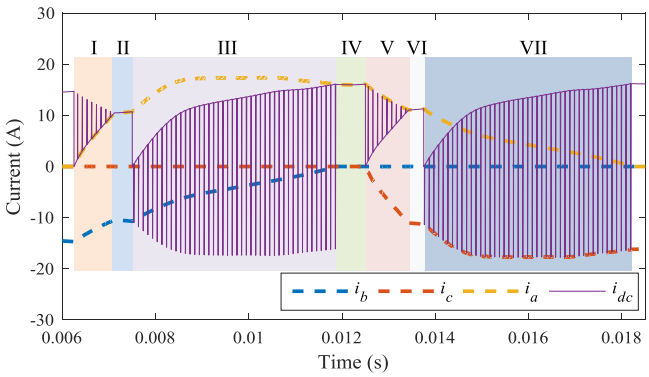

Fig. 16. Phase currents and bus current under SPV control with PWM signal injection.

According to the above analysis, the positive part of i_a can be reconstructed in all seven regions, and the negative part of i_a and the complete current of phase B and C can be reconstructed with the same method. Table II shows the normal switching logic, the switches used for PWM injection and the dc-link current with and without PWM injection under different conduction situations.

From Table II, it can be found that for overlapping conduction regions, the current of the incoming phase can be directly obtained without PWM injection, and the current of the other phase can be achieved by turning on one switch from the dual switch module with the PWM signal. For single-phase conduction regions, the combination of two phase currents can be directly obtained without PWM injection. The current of the conducting phase can be achieved by turning OFF the two active switches, and the current of the other phase can be obtained by simple operations as (14).

Fig. 16 shows the phase currents i_a, i_b, i_c, and bus current $i_{\rm dc}$ of the SRM under single-pulse voltage (SPV) control, and the PWM pulse signals are injected into the switches for phase current reconstruction, which can be reflected by the bus current. Taking phase A as an example, from the figure, it can be seen that i_a directly equals to $i_{\rm dc}$ in regions I, II, IV, and VI, so PWM signal injection is not required, while in regions III, V, and VII, PWM signal is applied. It should be noted that in the figure, the pulse is injected in region I, which is used to reconstruct the current of phase B.

The existing single sensor phase current reconstruction method for conventional SRM drive system just can obtain the

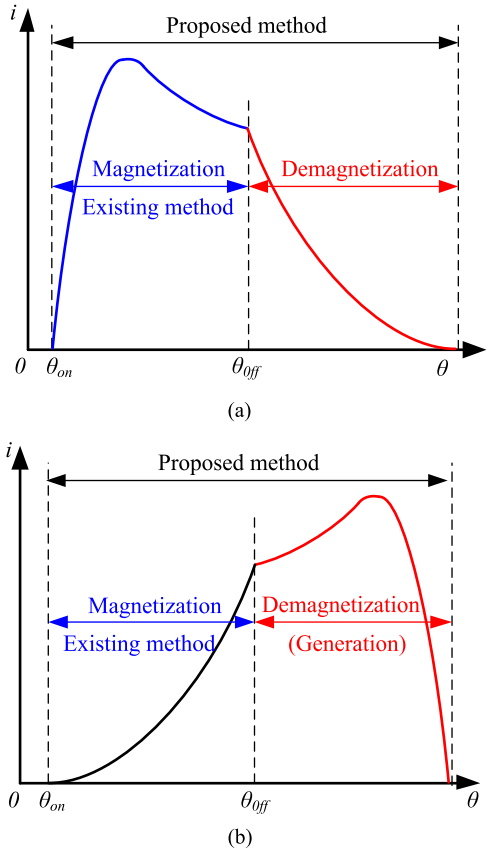

Fig. 17. Phase current under motoring and generating conditions with the indication of regions. (a) Motoring condition. (b) Generating condition.

phase current in the magnetization region, while the above proposed method can reconstruct the phase current in both magnetization and demagnetization regions. In other words, the proposed method can obtain the complete period phase current, which is very critical for the implementation of some methods, such as torque ripple reduction and rotor position estimation. Fig. 17 shows the different regions under both motoring and generating conditions, where $\theta_{\rm on}$ and $\theta_{\rm off}$ are the turn-on and turn-off angles, respectively.

IV. SIMULATION EVALUATION

A three-phase 12/8-pole SRM is employed to evaluate the proposed phase current reconstruction method, and its detailed specifications are presented in Table III, where the rated torque

TABLE III
DETAILED SPECIFICATIONS OF THE SRM PROTOTYPE

Rated power	1 kW	Stator outer diameter	120 mm
Rated speed	2000 r/min	Stack length	81 mm
Rated torque	4.8 N·m	Airgap length	0.15 mm

is obtained when the turn-on and turn-off angles equal to –3° and 18.5°, respectively. Based on the measured data of electromagnetic characteristics of the prototype, the simulation model is built in MATLAB with the method in [34].

The PWM signal is generated by the pulse generator block in Simulink. The simulation of open-loop control is implemented with the SPV control method, while the HCC scheme is carried out for speed closed-loop control based on the reconstructed phase currents. In all the simulations, the frequency and duty ratio of the injected PWM signal are set to 10 kHz and 0.9, respectively.

Fig. 18 compares the actual phase current i_a with its reconstructed value i_{are} under varied speeds, and the error $e_{ia} = i_a - i_{are}$, relative error $e_{ia*} = |i_a - i_{are}|/i_a \times 100\%$ and switching signals are shown as well. The SPV control method is adopted, and the turn-on and turn-off angles are set to 0° and 17°, respectively.

From Fig. 18, it can be found that e_{ia*} increases along with the rise of the speed. The proposed method is mainly based on PWM injection. The phase current is reconstructed at the beginning of each PWM pulse, and then maintained until the coming of the next pulse. For higher speed, fewer PWM pulses are included in one phase current period, and the errors resulted from the maintenance of the current will be larger. Furthermore, for a certain speed, big change ratio of phase current will cause a large error, such as shadowed regions A and B in Fig. 18(a). It should be noted that the change ratio of the current is also big before region A, but the error is tiny, which is because the current reconstruction in that region is not based on PWM injection, as illustrated in Table I. According to the above analysis, if smaller error is required, higher frequency PWM signal should be adopted.

In Fig. 19, the closed-loop speed control is carried out with HCC method, where the dc-link voltage and current hysteresis width are 96 V and 2 A, and the turn-on and turn-off angles are set to 0° and 18°, respectively. The reference speed rises from 1000 to 1500 r/min at 0.4 s, and the load torque is 2 N·m.

In Fig. 19, it can be found that the error also increases along with the rise of the speed, which is the same as the cases in Fig. 18. The reconstructed phase current is directly used for the closed-loop speed control, and the control performance is satisfactory, which indicates that it is feasible to implement speed control of SRM with the reconstructed phase current.

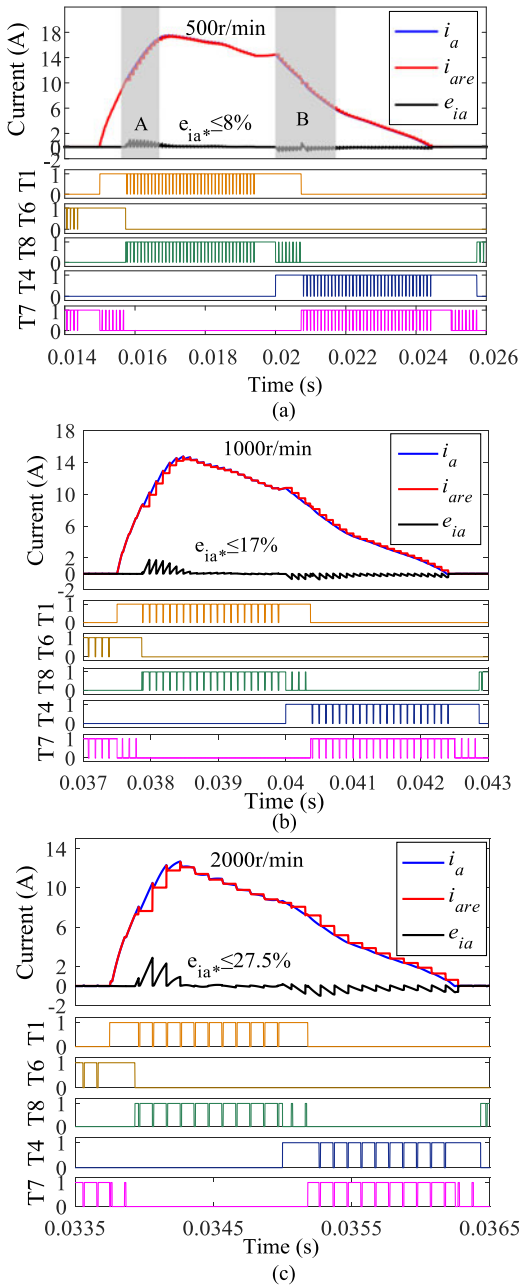

Fig. 18. Simulation current comparison with SPV control under different speeds. (a) Current comparison under 500 r/min. (b) Current comparison under 1000 r/min. (c) Current comparison under 2000 r/min.

V. EXPERIMENT EVALUATION

The phase current reconstruction method is evaluated by experiments with the aforementioned SRM prototype. The block diagram and photographs of the experimental test bench are illustrated in Figs. 20 and 21. The rotor position and speed are obtained with a resolver, and a magnetic powder break is used as the loading equipment. Table IV shows the chips and sensors used in the sampling and drive circuits.

In the test bench, with the reference and real speed, the reference current can be got by speed control. Then, the HCC is carried out with the reconstructed phase currents i_{are}, i_{bre}, and i_{cre} and reference current, and the hysteresis control signal is obtained. Based on the turn-on and turn-off angles $\theta_{\rm on}$ and $\theta_{\rm off}$, the rotor position, the hysteresis control signal and the injected PWM signal, the switching signal can be generated by logical processing. According to the switching signal, the switches in the power converter act correspondingly to control

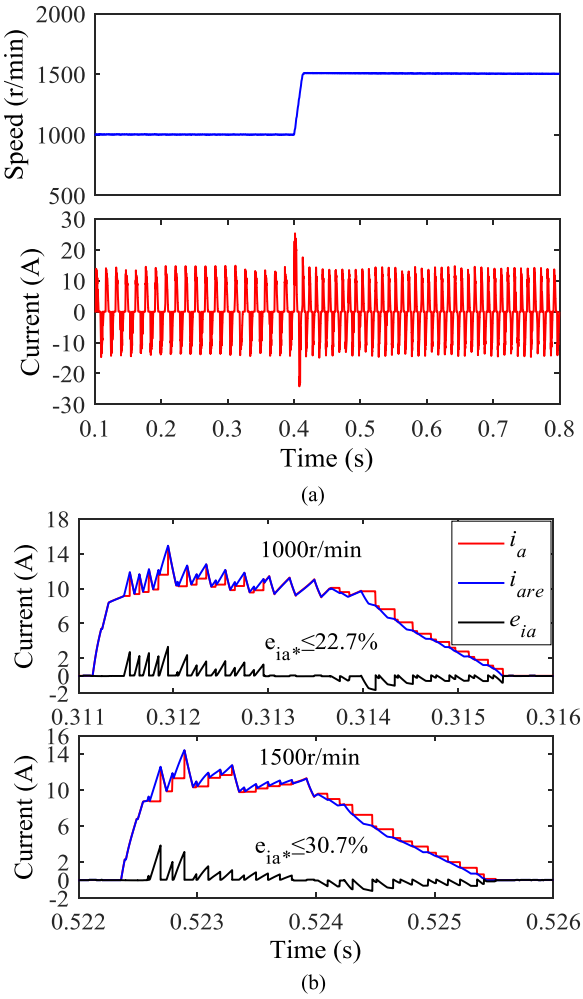

Fig. 19. Simulation results of closed-loop speed control based on HCC method with the reconstructed phase current. (a) Speed and reconstructed phase current. (b) Current comparison.

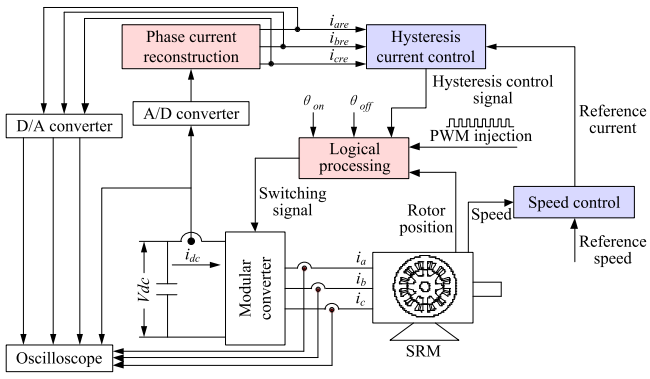

Fig. 20. Schematic diagram of the test bench.

the SRM. The bus current $i_{\rm dc}$ is measured by a current sensor and converted to digital signals by a 14-bit A/D converter, and the reconstructed phase currents are converted to analog form by a 14-bit D/A converter and compared with the measured phase currents i_a, i_b, and i_c in the oscilloscope. It should be noted that in Fig. 20, the function blocks in blue are implemented in digital signal processor (DSP), while red in field-programmable gate array (FPGA).

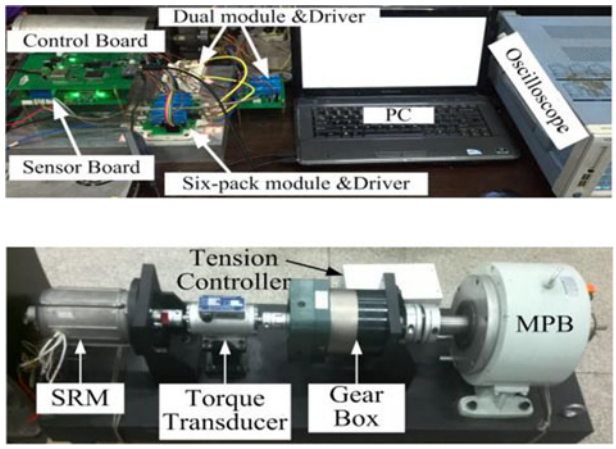

Fig. 21. Photographs of the test bench.

TABLE IV
ELEMENTS USED IN SAMPLING AND DRIVE CIRCUITS

Component	Selected model	Component	Selected model
DSP	TMS320F28335	D/A	AD9244
FPGA	EPM1270C5	Driver chip	QP12W05S-37
A/D	AD9767	Current sensor	LA25-NP

In Fig. 22, the actual and reconstructed currents of phase A with SPV control are compared under different speeds. The turn-on and turn-off angles are set to 0° and 17°, respectively. It should be noted that in all the experiments, the frequency and duty ratio of the injected PWM signal are set to 10 kHz and 0.9, respectively. In the figure, there are good agreements between the real and reconstructed phase currents, and the reconstruction errors increase along with the rise of the speed.

In Fig. 23, the closed-loop speed control is carried out based on HCC method with the reconstructed phase current, where the reference speed rises from 1500 to 2000 r/min and then falls to 1000 r/min, and the load torque is 2 N·m. The turn-on and turn-off angles are set to 0° and 18°, respectively. From the figure, it can be found that both the reconstruction and control performances are satisfactory.

It should be noted that following factors also can contribute to the reconstruction errors of the experiments.

1) The errors of A/D and D/A converters.
2) The switching characteristics of the switches, such as the turn-on and turn-off delay time.
3) The electromagnetic interference in measurement.

All the above simulations and experiments show that the proposed method can effectively reconstruct the phase currents of the SRM driven by the modular converter, and the closed-loop speed control under HCC method can be implemented with the reconstructed phase currents. To further analyze the influences of the reconstruction method on the performances of the SRM drive system. More experiments are carried out as follows.

Fig. 24 shows the torque speed curve comparison among AHB converter without reconstruction, modular converter with and without reconstruction. The power supply voltage is 96 V,

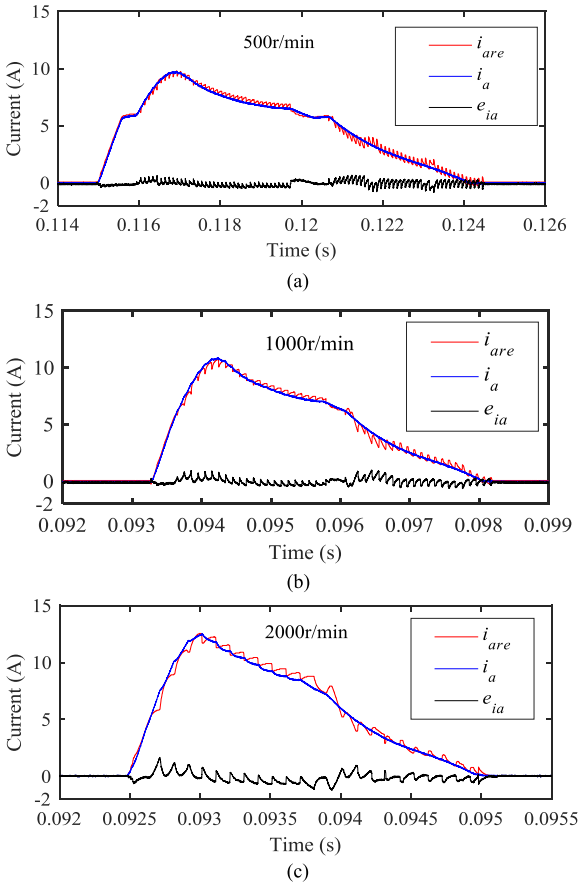

Fig. 22. Experimental current comparison with SPV control under different speeds. (a) Current comparison under 500 r/min. (b) Current comparison under 1000 r/min. (c) Current comparison under 2000 r/min.

the turn-on and turn-off angles are 0° and 18°, respectively, and the duty cycle of the PWM signal for current reconstruction is 0.95.

From the figure, it can be seen that the application of modular converter and phase current reconstruction method will slightly reduce the output torque, the reasons are as follows.

1) Compared with conventional AHB converter, in modular converter, there are some small regions where two phases are excited in series, and half of the dc-link voltage will be applied to each phase.
2) The injection of PWM signal for current reconstruction will slightly reduce the input electrical power, which is the common issue of the reconstruction method based on pulse injection.

For the SRM drive system with the modular converter, Fig. 25 compares the measured efficiency of the whole system with and without PWM injection, where the efficiency η is calculated by (15). From the figure, it can be found that the effect of the PWM injection on the system efficiency is very small. Furthermore, the influence of the PWM injection on current and torque ripple is also small, which can be found in the above simulation and experimental results

$$\eta = \frac{\text{output mechanical power}}{\text{input electrical power}} = \frac{T \cdot \omega}{U \cdot I} \tag{15}$$

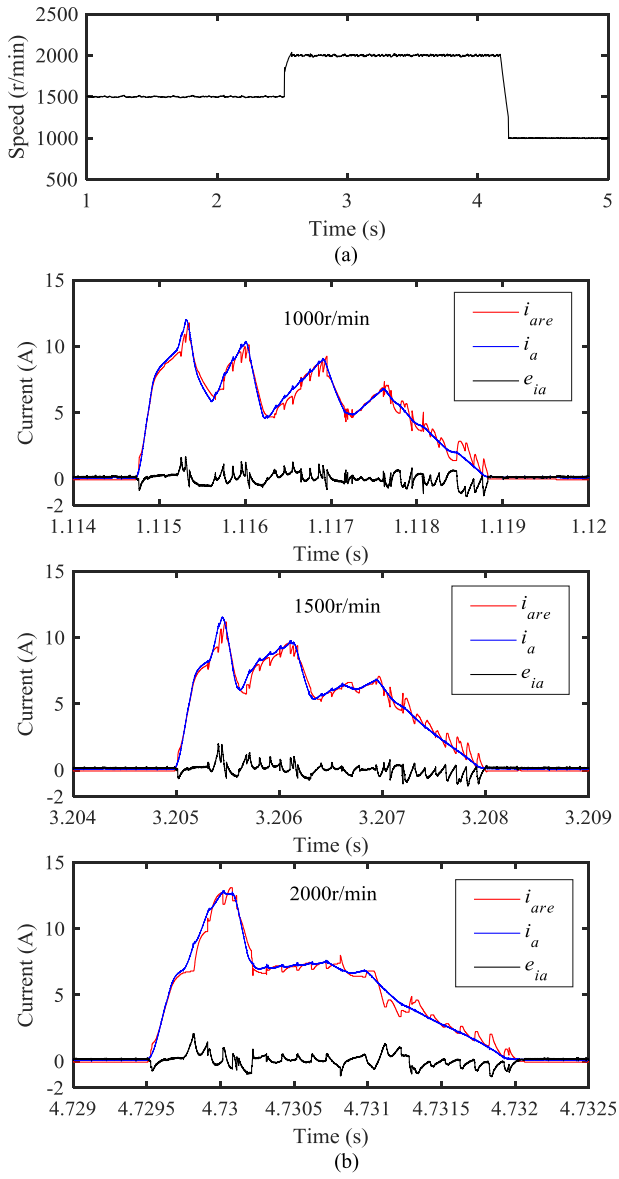

Fig. 23. Experimental results of closed-loop speed control based on HCC method with the reconstructed phase current. (a) Speed. (b) Current comparison.

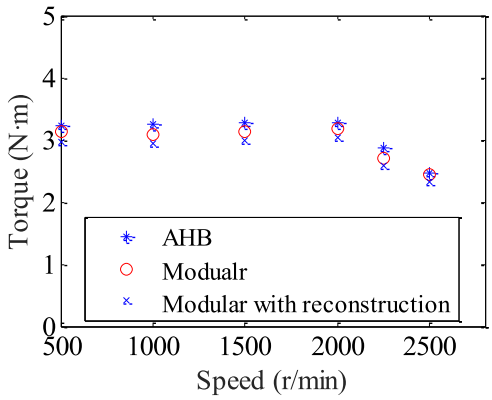

Fig. 24. Torque speed curve comparison.

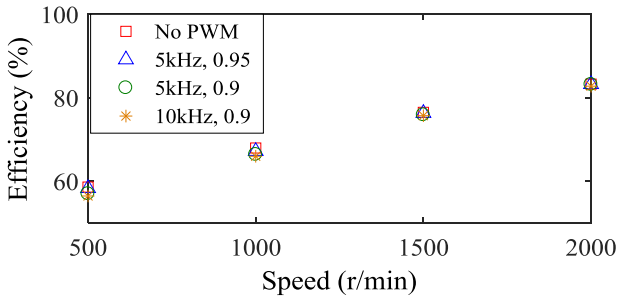

Fig. 25. System efficiency comparison with and without PWM injection.

where T, ω, U, I represent the torque, speed, bus voltage, and current, respectively.

VI. Conclusion

With the purpose of developing a highly integrated SRM drive system, a novel phase current reconstruction method with the modular power converter is proposed and evaluated. The method is based on the PWM signal injection, and the current of all the phases can be reconstructed from the sampled dc-link current. As the theoretical basis, detailed analysis of the current relationship with and without the PWM signal injection is presented, and several simulations and experiments are carried out to verify the effectiveness of the method.

The features of the proposed method can be summarized as follows.

1) It only needs one dc-link current sensor and one A/D channel and there is no special requirement on the current sensor, which further enhances the integration and reliability and reduces the cost of the considered modular converter.
2) It can obtain the complete period phase current, which is very critical for the implementation of some methods.
3) It dose not need change the structure of the converter, which retains all the advantages of the modular converter.
4) It only requires single high-frequency PWM signal, and the involved arithmetical operations are very simple, which makes the reconstruction convenient and guarantees the real-time performance.
5) It can obtain good reconstruction results, and its influences on the performances of the system, such as output torque and efficiency, are very small.

In practical applications, the performances of the proposed method are related to the speed of the machine and switching characteristics of the switches in the power converter. For higher speed application, the frequency of the injected PWM signal should be increased to guarantee satisfactory reconstruction accuracy, which requires better characteristics of the switches, such as higher switching frequency and shorter delay time.

References

[1] N. Jiao, W. Liu, T. Meng, J. Peng, and S. Mao, "Design and control of a two-phase brushless exciter for aircraft wound-rotor synchronous starter/generator in the starting mode," *IEEE Trans. Power Electron.*, vol. 31, no. 6, pp. 4452–4461, Jun. 2016.

[2] T. Kan, T.-D. Nguyen, J. C. Wjite, R. K. Malhan, and C. C. Mi, "A new integration method for an electric vehicle wireless charging system using LCC compensation topology: analysis and design," *IEEE Trans. Power Electron.*, vol. 32, no. 2, pp. 1638–1650, Feb. 2017.

[3] E. Levi, "Advances in converter control and innovative exploitation of additional degrees of freedom for multiphase machines," *IEEE Trans. Ind. Electron.*, vol. 63, no. 1, pp. 433–448, Jan. 2016.

[4] C. Gan, J. Wu, Y. Hu, S. Yang, W. Cao, and J. M. Guerrero, "New integrated multilevel converter for switched reluctance motor drives in plug-in hybrid electric vehicles with flexible energy conversion," *IEEE Trans. Power Electron.*, vol. 32, no. 5, pp. 3754–3766, May 2017.

[5] C. E. Capovilla, I. R. S. Casella, A. J. S. Filho, T. A. Dos, S. Barros, and E. R. Filho, "Performance of a direct power control system using coded wireless OFDM power reference transmissions for switched reluctance aerogenerators in a smart grid scenario," *IEEE Trans. Ind. Electron.*, vol. 62, no. 1, pp. 52–61, Jan. 2015.

[6] Q. Yu, B. Bilgin, and A. Emadi, "Loss and efficiency analysis of switched reluctance machines using a new calculation method," *IEEE Tran. Ind. Electron.*, vol. 62, no. 5, pp. 3072–3080, May 2015.

[7] L. Szabo and M. Ruba, "Segmental stator switched reluctance machine for safety-critical applications," *IEEE Trans. Ind. Appl.*, vol. 48, no. 6, pp. 2223–2229, Nov./Dec. 2012.

[8] M. Ruba and D. Fodorean, "Development of a complete motor-drive solution for light EV based on a SRM," in *Proc. Int. Conf. Expo. Elect. Power Eng.*, Dec. 2016, pp. 197–204.

[9] J. W. Ahn, S. G. Oh, J. W. Moon, and Y. M. Hwang, "A three-phase switched reluctance motor with two-phase excitation," *IEEE Trans. Ind. Appl.*, vol. 35, no. 5, pp. 1067–1075, Sep. 1999.

[10] X. Liu, Z. Q. Zhu, M. Hasegawa, A. Pride, and R. Deohar, "Performance comparison between unipolar and bipolar excitations in switched reluctance machine with sinusoidal and rectangular waveforms," *Energy Convers. Congr. Expo.*, vol. 47, no. 10, pp. 1590–1595, Sep. 2011.

[11] X. Liu, Z. P. Pan, and Z. Q. Zhu, "Analysis of average torque in switched reluctance motor with unipolar and bipolar excitations based on an improved Fourier series model," *IEEE Veh. Power Propulsion Conf.*, Sep. 2010, pp. 1–6.

[12] J. D. Widmer, B. C. Mecrow, C. M. Spargo, R. Martin, and T. Celik, "Use of a 3 phase full bridge converter to drive a 6 phase switched reluctance machine," in *Proc. 6th IET Int. Conf. Power Electron., Mach. Drives*, Mar. 2012, pp. 1–6.

[13] W. Cai and F. Yi, "An integrated multiport power converter with small capacitance requirement for switched reluctance motor drive," *IEEE Trans. Power Electron.*, vol. 31, no. 4, pp. 3016–3026, Apr. 2016.

[14] Z. Grbo and S. Vukosavic, "Cost-optimized switched reluctance motor drive with bipolar currents," *Elect. Eng.*, vol. 89, no. 3, pp. 183–191, Jan. 2007.

[15] S. Song, Z. Xia, Z. Zhang, and W. Liu, "Control performance analysis and improvement of a modular power converter for 3-phase SRM with y-connected windings and neutral line," *IEEE Trans. Ind. Electron.*, vol. 63, no. 10, pp. 6020–6030, Oct. 2016.

[16] K.-W. Hu, Y.-Y. Chen, and C.-M. Liaw, "A reversible position sensorless controlled switched-reluctance motor drive with adaptive and intuitive commutation tunings," *IEEE Trans. Power Electron.*, vol. 30, no. 7, pp. 3781–3793, Jul. 2015.

[17] J. Ye, B. Bilgin, and A. Emadi, "Elimination of mutual flux effect on rotor position estimation of switched reluctance motor drives," *IEEE Trans. Power Electron.*, vol. 30, no. 3, pp. 1499–1512, Mar. 2015.

[18] S. Song, L. Ge, and Z. Zhang, "Accurate position estimation of SRM based on optimal interval selection and linear regression analysis," *IEEE Trans. Ind. Electron.*, vol. 63, no. 6, pp. 3467–3478, Jun. 2016.

[19] E. Ofori, T. Husain, Y. Sozer, and I. Husain, "A pulse injection based sensorless position estimation method for a switched reluctance machine over a wide speed range," *IEEE Trans. Ind. Appl.*, vol. 51, no. 5, pp. 3867–3876, Sep./Oct. 2015.

[20] F. Blaabjerg, J. K. Pedersen, U. Jaeger, and P. Thoegersen, "Single current sensor technique in the DC link of three-phase PWM-VS inverters: A review and a novel solution," *IEEE Trans. Ind. Appl.*, vol. 33, no. 5, pp. 1241–1253, Sep./Oct. 1997.

[21] Y. Gu, F. Ni, D. Yang, and H. Liu, "Switching-state phase shift method for three-phase current reconstruction with a single DC-link current sensor," *IEEE Trans. Ind. Electron.*, vol. 58, no. 11, pp. 5186–5194, Nov. 2011.

[22] B. Metidji, N. Taib, L. Baghli, T. Rekioua, and S. Bacha, "Phase current reconstruction using a single current sensor of three-phase AC motors fed by SVM-controlled direct matrix converters," *IEEE Trans. Ind. Electron.*, vol. 60, no. 12, pp. 5497–5505, Dec. 2013.

[23] B. Saritha and P. Janakiraman, "Sinusoidal three-phase current reconstruction and control using a DC-Link current sensor and a curve-fitting observer," *IEEE Trans. Ind. Electron.*, vol. 54, no. 5, pp. 2657–2664, Oct. 2007.
[24] X. Li, S. Dusmez, B. Akin, and K. Rajashekara, "A new SVPWM for the phase current reconstruction of three-phase three-level T-type converters," *IEEE Trans. Power Electron.*, vol. 31, no. 3, pp. 2627–2637, Mar. 2016.
[25] H. Lu, X. Cheng, W. Qu, and S. Sheng, "A three-phase current reconstruction technique using single DC current sensor based on TSPWM," *IEEE Trans. Power Electron.*, vol. 29, no. 3, pp. 1542–1550, Mar. 2014.
[26] P. C. Kjaer and G. Gallegos-Lopez, "Single-sensor current regulation in switched reluctance motor drives," *IEEE Trans. Ind. Appl.*, vol. 34, no. 3, pp. 444–451, May/Jun. 1998.
[27] C. Gan, J. Wu, S. Yang, and Y. Hu, "Phase current reconstruction of switched reluctance motors from dc-link current under double high-frequency pulses injection," *IEEE Trans. Ind. Electron.*, vol. 62, no. 5, pp. 3265–3276, May 2015.
[28] C. Gan, J. Wu, Q. Sun, S. Yang, Y. Hu, and L. Jin, "Low-cost direct instantaneous torque control for switched reluctance motors with bus current detection under soft-chopping mode," *IET Elect. Power Appl.*, vol. 9, no. 3, pp. 482–490, Mar. 2016.
[29] P. Dúbravka, P. Rafajdus, P. Makyš, and L. Szabó, "Control of switched reluctance motor by current profiling under normal and open phase operating condition," *IET Elect. Power Appl.*, vol. 11, no. 4, pp. 548–556, Apr. 2017.
[30] G. Han, H. Chen, X. Shi, and Y. Wang, "Phase current reconstruction strategy for switched reluctance machines with fault-tolerant capability," *IET Elect. Power Appl.*, vol. 11, no. 3, pp. 399–411, Mar. 2017.
[31] M. Barnes and C. Pollock, "Power electronic converters for switched reluctance drives," *IEEE Trans. Power Electron.*, vol. 13, no. 6, pp. 1100–1111, Nov. 1998.
[32] X. D. Xue, K. W. E. Cheng, and Y. J. Bao, "Control and integrated half bridge to winding circuit development for switched reluctance motors," *IEEE Trans. Ind. Inf.*, vol. 10, no. 1, pp. 109–116, Feb. 2014.
[33] K. Tungpimolrut, S. Kachapornkul, P. Jitkreeyarn, P. Somsiri, N. Chayopitak, and C. Akira, "Bipolar excitation for double three-phase full bridge converter based three-phase switched reluctance motor drive system," in *Proc. 39th Annu. Conf. IEEE Ind. Electron. Soc.*, Nov. 2013, pp. 2626–2631.
[34] S. Song, L. Ge, S. Ma, M. Zhang, and L. Wang, "Accurate measurement and detailed evaluation of static electromagnetic characteristics of switched reluctance machines," *IEEE Trans. Instrum. Meas.*, vol. 64, no. 3, pp. 704–714, Mar. 2015.

Shoujun Song (M'08–SM'16) received the B.S. and M.S. degrees from the Northwestern Polytechnical University, Xi'an, China, in 2003 and 2006, respectively, and the Dr.-Ing. degree from the Technical University of Berlin, Berlin, Germany, in 2009, all in electrical engineering.

He is currently an Associate Professor with the Department of Electrical Engineering, Northwestern Polytechnical University. His research interests include electric machines and drives with emphasis on switched reluctance machine design and control.

Zekun Xia (S'17) received the B.S. and M.S. degrees in electrical engineering from the Northwestern Polytechnical University, Xi'an, China, in 2014 and 2017, respectively. He is currently working toward the Ph.D. degree in electrical engineering at the McMaster Institute for Automotive Research and Technology, McMaster University, Hamilton, ON, Canada.

His main research interests include optimal control methods for electric machines and power electronics.

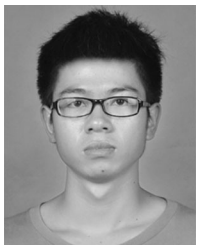

Gaoliang Fang received the B.S. degree, in 2015, in electrical engineering from the Northwestern Polytechnical University, Xi'an, China, where he is currently working toward the M.S. degree in electrical engineering.

His main research interests include advanced control of switched reluctance machines.

Ruiqing Ma (M'05) received the B.S., M.S., and Ph.D. degrees in electrical engineering from the Northwestern Polytechnical University, Xi'an, China, in 1985, 1988, and 2007, respectively.

He is currently a Professor with the Department of Electrical Engineering, and the Deputy Director of the Institute of the Rare Earth Permanent Magnet Electrical Machines and Control Technology, Northwestern Polytechnical University. Since 1993, he has been teaching and conducting research on electric machines and power converters with Northwestern Polytechnical University. His research interests include permanent magnet electric machines, power converters, and renewable energy systems.

Weiguo Liu (M'99–SM'07) received the B.S. degree in electrical machine engineering from the Huazhong University of Science and Technology, Wuhan, China, and the M.S. degree in electrical engineering and the Ph.D. degree in control theory and control engineering from the Northwestern Polytechnical University, Xi'an, China, in 1982, 1988, and 1999, respectively.

He is currently a Professor with the Department of Electrical Engineering, Northwestern Polytechnical University, Xi'an, China, and a Guest Professor with the University of Federal Defense, Munich, Germany. He is the Director of the Institute of Rare Earth Permanent Magnet Electrical Machines and Control Technology, Northwestern Polytechnical University. His research interests include brushless dc machines, PM synchronous machines, and induction machines.

Prof. Liu was the Chairman of the Organizing Committee of the 32nd Chinese Control Conference, Xi'an, China, in July 2013.